

Pressure and strain tuning of the alternating bilayer-trilayer Ruddlesden-Popper nickelate: crystal and electronic structure

Huan Wu,¹ Yi-Feng Zhao,¹ and Antia S. Botana¹

¹*Department of Physics, Arizona State University, Tempe, AZ 85287, USA*

(Dated: March 18, 2026)

We use first-principles calculations to investigate the crystal and electronic structure of the hybrid bilayer-trilayer Ruddlesden-Popper (RP) nickelate $\text{La}_7\text{Ni}_5\text{O}_{17}$ under hydrostatic pressure and biaxial compressive strain. By analyzing the irreducible representations of the dynamically unstable phonon modes in the high-symmetry $P4/mmm$ structure, we identify a dynamically stable lower-symmetry $C2/c$ structure containing octahedral tilts. The application of both pressure and compressive strain tends to suppress the octahedral tilts, effectively tetragonalizing the structure, in analogy with the conventional RPs. The electronic structure under hydrostatic pressure and strain has similarities, but it differs in the position of the d_{z^2} bonding band from the trilayer block. This band crosses the Fermi level at a pressure of 30 GPa, but it remains below it for any level of compressive strain. This strain-induced modification mirrors the electronic structure changes observed in the conventional bilayer nickelate.

I. INTRODUCTION

The observation of superconductivity under pressure in the parent Ruddlesden-Popper (RP) $R_{n+1}\text{Ni}_n\text{O}_{3n+1}$ nickelates [1–5] opened a new avenue for the study of high- T_c superconductivity. The materials in this family are characterized by the presence of n - NiO_6 perovskite layers separated by rocksalt RO blocks along the c -axis [6]. The first signatures of superconductivity were reported in the bilayer ($n = 2$) RP nickelate $\text{La}_3\text{Ni}_2\text{O}_7$ [1–3] with a $T_c \sim 80$ K within a pressure range of ~ 14.0 to 43.5 GPa [1]. Concomitant with the emergence of superconductivity, a structural transition from orthorhombic $Amam$ at ambient pressure to either $Fmmm$ or tetragonal $I4/mmm$ symmetry at 14.0 GPa has been reported [1, 7, 8]. This transition is associated to a suppression of octahedral tilts, with the Ni-O-Ni bond angle changing from 168° to 180° . The $n = 3$ member $\text{La}_4\text{Ni}_3\text{O}_{10}$ also exhibits superconductivity when pressurized (albeit with lower $T_c \sim 40$ K), and a similar structural transition from monoclinic $P2_1/a$ at ambient pressure to tetragonal $I4/mmm$ at 13–15 GPa [4, 5, 9–11]. Similar to the $n = 2$ member, this transition is also associated with the change in the Ni-O-Ni bond angle across the apical oxygens from 166° to 180° . A similar structural transition is observed in $\text{La}_3\text{Ni}_2\text{O}_7$ when grown in thin film form upon compressive strain, wherein superconductivity has also been observed [12–17]. The electronic structure of both the bilayer and trilayer materials is characterized by the active role of bands of $d_{x^2-y^2}$ and d_{z^2} character at the Fermi level. Many studies have suggested that the straightening of the Ni-O-Ni bond angle along the c -axis with pressure is related with the emergence of superconductivity due to associated enhancement in d_{z^2} inter-layer coupling [18–31].

Recently, new hybrid RP nickelate phases $\text{La}_{n+1}\text{Ni}_n\text{O}_{3n+1} \cdot \text{La}_{m+1}\text{Ni}_m\text{O}_{3m+1}$ $n > m$ have been reported [32]. The first one to be discovered is a polymorph of $\text{La}_3\text{Ni}_2\text{O}_7$ [33–37] whose structure is formed by alternating single-layer ($m=1$) and trilayer

($n = 3$) blocks forming a 1313 configuration. Superconductivity in this new $\text{La}_3\text{Ni}_2\text{O}_7$ -1313 polymorph has also been reported under pressure with a T_c as high as that of the conventional bilayer (2222) counterpart [35–37]. Superconductivity under pressure has also been reported in the single-layer ($m=1$) +bilayer ($n=2$) RP nickelate $\text{La}_5\text{Ni}_3\text{O}_{11}$ with a $T_c \sim 60$ K [38]. In both of these systems, the leading space group symmetry reported at ambient pressure is $Cmmm$, in which there is no octahedral tilting at ambient pressure. There is, however, evidence in the in-lab X-ray diffraction data of weak superlattice reflections that could lead to tilted octahedra [33, 36, 39]. The electronic structure of these hybrid phases has been scrutinized, and it exhibits some similarities with the $\text{La}_3\text{Ni}_2\text{O}_7$ -2222 counterpart, while there are discrepancies about the single-layer block being in a Mott-insulating regime [36, 40–43]. Recently, superconductivity in these two hybrid phases upon compressive strain provided by a SrLaAlO_4 (SLAO) substrate has been explored: while the 1212 hybrid is also superconducting in thin film form, the 1313 phase is not [44].

In order to identify strategies to emulate and surpass the superconducting properties of the existing superconducting RP nickelates, other members of the hybrid family and the effects of pressure and strain on their electronic structure can be scrutinized. As the recent results described above seem to point towards the need for a bilayer structural motif in RPs to get superconductivity (and a higher T_c), an obvious choice is represented by the bilayer ($m=2$) +trilayer ($n=3$) counterpart $\text{La}_7\text{Ni}_5\text{O}_{17}$ -2323. This phase (not yet experimentally realized) has been scrutinized under pressure in a couple of theoretical works [45, 46], but no comparison with strain has been performed, and the ambient-pressure structure has not yet been carefully analyzed. The existing electronic structure calculations under pressure show the emergence of extra d_{z^2} states at the Fermi level under pressure associated with the trilayer block, and a leading s^\pm -superconducting

symmetry with similar pairing strength to that obtained previously for $\text{La}_3\text{Ni}_2\text{O}_7$ -2222 [45].

Here, we perform first-principles calculations to shed light on the structural and electronic structure evolution of the hybrid bilayer-trilayer RP nickelate $\text{La}_7\text{Ni}_5\text{O}_{17}$ -2323 upon hydrostatic pressure and strain. We start by investigating the structural stability of the higher-symmetry $P4/mmm$ structure at ambient pressure and explore the symmetry connections with other space groups. Our lattice dynamics calculations reveal that the $P4/mmm$ phase exhibits multiple dynamical instabilities. Using group theory analysis, we find that the distortions associated with the irreducible representations (irreps) of the unstable phonon branches could transform the $P4/mmm$ structure into a $C2/c$ space group, containing octahedral tilts. Under pressure and compressive strain, these octahedral tilts tend to be suppressed, tetragonalizing the structure. The electronic structure we find under pressure (~ 30 GPa) is similar to that reported in the literature. Upon strain, the electronic structure differs as the bonding d_{z^2} trilayer band emerging at the Fermi level upon pressure is pushed below the Fermi level upon compressive strain. This change in the electronic structure is analog to that reported in compressively strained bilayer $\text{La}_3\text{Ni}_2\text{O}_7$ -2222, making it important to understand whether the related corner pockets are important to develop superconductivity.

II. COMPUTATIONAL METHODS

The density functional theory (DFT) calculations are performed using plane-wave basis set as implemented in Quantum ESPRESSO [47, 48]. The exchange-correlation is described by the Perdew–Burke–Ernzerhof functional within the generalized gradient approximation [49]. Ultrasoft pseudopotentials are employed [50]. The kinetic energy cutoffs for the wavefunctions and for the charge density and potential are set to 80 Ry and 640 Ry, respectively. Brillouin zone integration is performed using Monkhorst-Pack \mathbf{k} -point grids of $12 \times 12 \times 2$ and $8 \times 8 \times 2$ for $P4/mmm$ and $C2/c$ structures, respectively. All structures are relaxed until the interatomic forces are less than 10^{-4} Ry/bohr. The Fermi energy and Fermi surface are determined from a \mathbf{k} -point grid of $24 \times 24 \times 2$. The phonon dispersions of the $P4/mmm$ structure are calculated using ALAMODE [51]. The interatomic force constants are derived by fitting the irreducible displacement-force set, for which the interatomic forces are calculated by DFT on a $2 \times 2 \times 1$ 116-atom supercell with a $6 \times 6 \times 2$ Monkhorst-Pack \mathbf{k} -point grid.

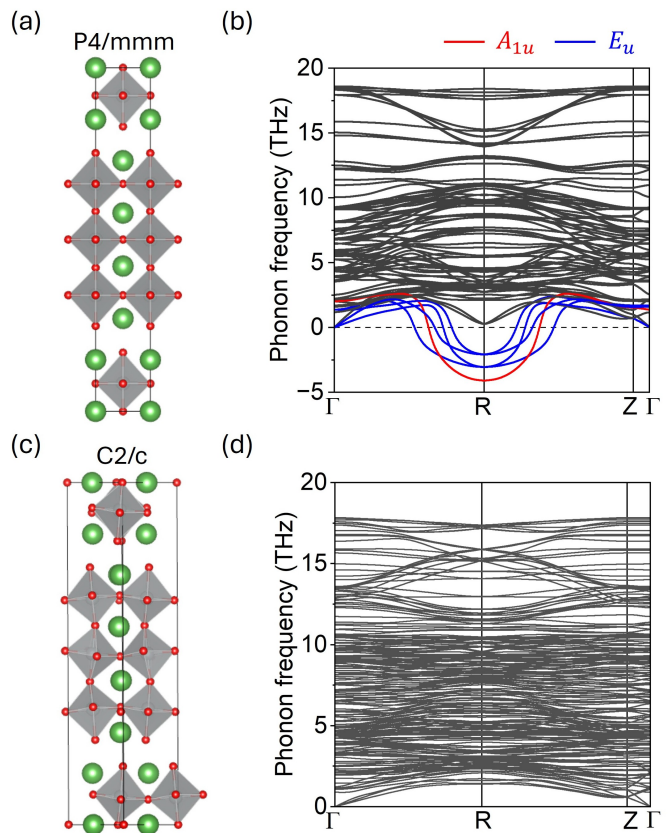


FIG. 1. Crystal structure of $\text{La}_7\text{Ni}_5\text{O}_{17}$ -2323 and phonon dispersion relation. The high-symmetry space group $P4/mmm$ (a), that displays no octahedral tilts, gives rise to unstable phonon modes (b). The structure obtained by applying distortions according to the irreducible representation of those modes (and relaxing) has $C2/c$ symmetry and contains octahedral tilts (c), characteristic of perovskite nickelates. The phonon dispersion of the $C2/c$ structure exhibits no imaginary frequencies (d), confirming its dynamic stability. Spheres in green, gray, and red in panels (a,c) represent the La, Ni, and O atoms, respectively.

III. RESULTS

A. Structural stability at ambient pressure

We start by analyzing the dynamical stability of the crystal structure with higher symmetry at ambient pressure ($P4/mmm$) for the bilayer-trilayer hybrid nickelate $\text{La}_7\text{Ni}_5\text{O}_{17}$, studying its phonon dispersion (see Fig. 1(a,b)). As shown in Fig. 1(a), in tetragonal $P4/mmm$ symmetry, all Ni–O–Ni bond angles are 180° , indicating the absence of both out-of-plane tilting and in-plane rotations of the NiO_6 octahedra between adjacent layers. The phonon dispersion in Fig 1(b) shows five modes exhibit imaginary frequencies at the R-point of the Brillouin zone. The lowest-energy mode corresponds to an A_{1u} irreducible representation, while the remaining four modes, forming two pairs of degenerate modes at the R point, belong to the E_u irreducible representation.

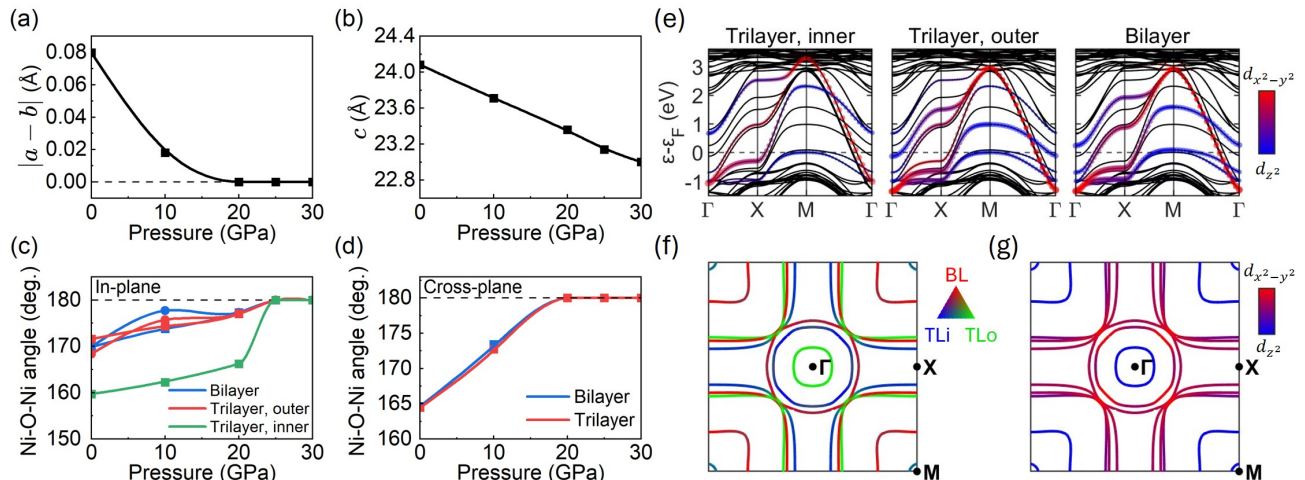


FIG. 2. Evolution of the structural parameters of $\text{La}_7\text{Ni}_5\text{O}_{17-2323}$ under hydrostatic pressure and its electronic structure at 30 GPa. (a-d) Pressure-dependent evolution of (a) the absolute difference between in-plane lattice constants $|a - b|$; (b) the cross-plane lattice constant c ; (c) the in-plane Ni-O-Ni bond angle; and (d) the cross-plane Ni-O-Ni bond angle. (e) Electronic band structure at 30 GPa, with colors representing contributions from $d_{x^2-y^2}$ (red) and d_{z^2} (blue) orbitals of the Ni in the inner layer of the trilayer (left), outer layer of the trilayer (middle), and bilayer (right). (f,g) Fermi surface cutoff at the $k_z = 0$ plane, with colors representing (f) contributions from the inner layer of the trilayer (TLi), outer layer of the trilayer (TLo), and bilayer (BL) Ni sites, and (g) contributions from the $d_{x^2-y^2}$ (red) and d_{z^2} (blue) orbitals of Ni.

The distorted structures obtained by displacing atoms from their equilibrium positions according to the phonon eigenvectors of these unstable modes can be seen in Appendix A. The modes with A_{1u} symmetry correspond to an in-plane distortion of NiO_6 octahedra, whereas the E_u ones represent tilting of the NiO_6 octahedra.

To identify the dynamically stable structure at ambient pressure, we generate a distorted structure on a $2 \times 2 \times 2$ supercell by combining the distortions of the A_{1u} mode and the two nondegenerate E_u modes. After relaxation, this distorted structure converged to a $C2/c$ space group, as shown in Fig. 1(c). The phonon dispersion of the $C2/c$ structure exhibits no imaginary frequencies, confirming its dynamical stability (see Fig. 1(d)). Hence, our analysis of the unstable phonon branches in the higher-symmetry structure for $\text{La}_7\text{Ni}_5\text{O}_{17-2323}$ ($P4/mmm$) shows that it can transform into a dynamically-stable lower-symmetry $C2/c$ structure through distortions associated with the irreps of unstable modes at the R point. This hybrid structure, akin to the conventional bilayer and trilayer compounds, contains octahedral tilts with Ni-O-Ni bond angles across the apical oxygens between 160 and 170° (see Fig. 2).

B. Crystal structure and electronic structure under pressure

After analyzing the structural stability of $\text{La}_7\text{Ni}_5\text{O}_{17}$ at ambient pressure, we now focus on its evolution with pressure. The changes under pressure for the c lattice constant, the difference $|a-b|$ between the in-plane lattice

constants, and the Ni-O-Ni bond angle across the apical/plantar oxygens (plotted separately for the bilayer and trilayer blocks) are shown in Fig. 2(a-d). The starting (ambient pressure) structure is the $C2/c$ phase described in the previous section. The a and b lattice parameters become equal at ~ 20 GPa, resulting in a tetragonalized crystal structure. Concomitantly, the Ni-O-Ni apical bond angles (cross-plane angles) straighten to 180° at 20 GPa, while for the planar angles, the transition to 180° is slower and only reached at 25 GPa. As expected, under hydrostatic pressure, all Ni-O bonds (both in-plane and cross-plane) are reduced as pressure is applied. In the context of energetics, a $P4/mmm$ structure can also be seen to become more stable at 30 GPa. These findings are consistent with the phonon calculations where, with increasing pressure, the soft phonon branches harden, leading to a dynamically stable crystal structure with $P4/mmm$ symmetry at ~ 30 GPa (see Appendix B).

We next describe the electronic structure of $\text{La}_7\text{Ni}_5\text{O}_{17}$ under pressure (see Fig. 2(e-g)), where superconductivity could emerge as pointed out by previous theory work [45]. We focus on a 30 GPa pressure value, where the structure has fully transitioned to a tetragonal phase. A formal valence count renders an (average) $\text{Ni}^{2.6+}$ valence corresponding to a $d^{7.4}$ filling. With the t_{2g} orbitals being fully occupied, that leaves 1.4 e_g electrons per Ni to fill the e_g orbitals. As a reflection of this filling, the electronic structure of $\text{La}_7\text{Ni}_5\text{O}_{17}$ shows bands of both d_{z^2} and $d_{x^2-y^2}$ character crossing the Fermi level. These states are highly hybridized with O- p states. Like in the isolated/conventional trilayer and bilayer compounds, the d_{z^2} orbitals are split into a molecular orbital combina-

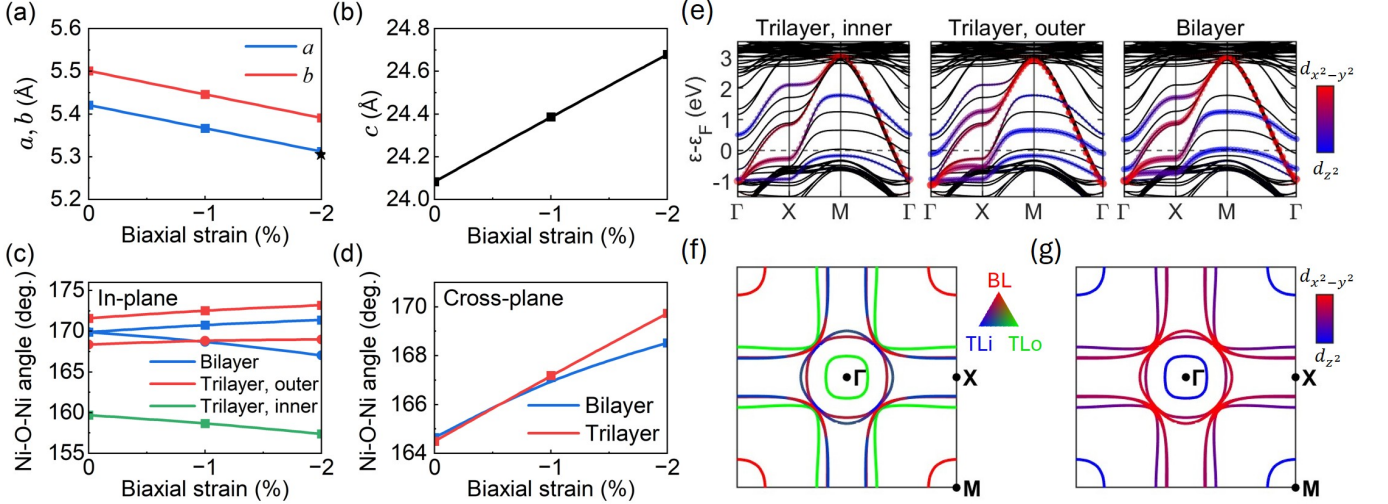


FIG. 3. Evolution of the structural parameters of $\text{La}_7\text{Ni}_5\text{O}_{17-2323}$ under biaxial compressive strain and its electronic structure at a -2% biaxial strain. (a-d) Strain-dependent evolution of (a) the in-plane lattice constants with the symmetry starting as $C2/c$; (b) the cross-plane lattice constant c ; (c) the in-plane Ni-O-Ni bond angle; and (d) the cross-plane Ni-O-Ni bond angle. The star on the right y-axis of (a) marks the in-plane lattice constant at 15 GPa. (e) Electronic band structure at -2% biaxial strain, with colors representing contributions from $d_{x^2-y^2}$ (red) and d_{z^2} (blue) orbitals of the Ni in the inner layer of the trilayer (left), outer layer of the trilayer (middle), and bilayer (right). (f,g) Fermi surface cutoff at the $k_z = 0$ plane, with colors representing (f) contributions from the inner layer of the trilayer (TLi), outer layer of the trilayer (TLo), and bilayer (BL) Ni sites, and (g) contributions from the $d_{x^2-y^2}$ (red) and d_{z^2} (blue) orbitals of Ni.

tion of bonding-antibonding states (bilayer block) and of bonding-nonbonding-antibonding states (trilayer block). The bonding d_{z^2} orbital from the bilayer clearly crosses the Fermi level at the M point of the Brillouin zone, giving rise to a corner pocket in the Fermi surface. The bonding d_{z^2} orbital from the trilayer barely crosses at 30 GPa, giving rise to a very small hole pocket also at the zone corner. As described before [45, 46] the emergence of this trilayer band at the Fermi level is the most important change with pressure (in addition to the expected bandwidth increase). While the size of this pocket at 30 GPa is smaller in our calculations, in prior work using random phase approximation (RPA) calculations, its emergence was deemed to be important for superconductivity [45]. The gap distribution found in this work is very similar to that of the isolated trilayer – but with an enhanced pairing strength. We note, however, that this pocket is fragile and the introduction of an on-site Coulomb repulsion U (as well as a lower pressure) can push the bonding trilayer band below the Fermi level (see Appendices C and D). The d_{z^2} bands higher in energy (above the Fermi level) are the nonbonding one from the trilayer (with only contributions from the outer Ni), the antibonding one from the bilayer, and finally the antibonding band from the trilayer Nis. Ultimately, the low-energy physics in the DFT nonmagnetic bands seems to be a combination of both of the constituent structural blocks (with some small band shifts).

The derived hoppings at 30 GPa further reinforce this picture of superposition of trilayer and bilayer physics in $\text{La}_7\text{Ni}_5\text{O}_{17}$ (see Table I). The dominant hoppings ob-

TABLE I. Hopping parameters (in eV) for $\text{La}_7\text{Ni}_5\text{O}_{17}$, bilayer $\text{La}_3\text{Ni}_2\text{O}_7$, and trilayer $\text{La}_4\text{Ni}_3\text{O}_{10}$ under ambient and high pressure (15 and 30 GPa), as well as upon a -2% compressive strain.

	Ni	hybrid bilayer+trilayer				bilayer		trilayer	
		0 GPa	15 GPa	30 GPa	-2%	30 GPa	-2%	30 GPa	-2%
t_{\perp}^z	TL	-0.595	-0.639	-0.677	-0.606			-0.676	-0.605
	BL	-0.581	-0.627	-0.664	-0.591	-0.665	-0.596		
t_{\parallel}^x	TLi	-0.441	-0.479	-0.510	-0.479			-0.512	-0.480
	TLo	-0.442	-0.478	-0.507	-0.476			-0.507	-0.474
	BL	-0.438	-0.475	-0.507	-0.470	-0.507	-0.475		
t_{\parallel}^{xz}	TLi	0.240	0.261	0.277	0.244			0.280	0.245
	TLo	0.229	0.250	0.265	0.225			0.269	0.227
	BL	0.223	0.242	0.258	0.212	0.255	0.208		

tained for the “isolated” conventional bilayer $\text{La}_3\text{Ni}_2\text{O}_7$ and trilayer $\text{La}_4\text{Ni}_3\text{O}_{10}$ are almost identical to those derived for the 2323 material at 30 GPa – and these values significantly increase from their ambient pressure counterparts. Such dominant hoppings are t_{\perp}^z that defines the overlap between the d_{z^2} orbitals via the O- p_z orbitals (~ 0.6 eV at 30 GPa), the nearest-neighbor hopping for the $d_{x^2-y^2}$ orbitals $t_{\parallel}^x \sim 0.5$ eV under pressure, and the hybridization in-plane between $d_{x^2-y^2}$ and d_{z^2} orbitals $t_{\parallel}^{xz} \sim 0.2$ eV also at 30 GPa.

C. Crystal structure and electronic structure under strain

We continue by looking at the structural data for $\text{La}_7\text{Ni}_5\text{O}_{17}$ under compressive strain (see Fig. 3(a-d)). As mentioned above, superconductivity has been achieved in bilayer $\text{La}_3\text{Ni}_2\text{O}_7$, as well as in the single-layer bilayer hybrid $\text{La}_5\text{Ni}_3\text{O}_{11}$ thin films upon a -2% compressive strain by growing thin films on SLAO [12–17, 44]. The relationship between the emergence of superconductivity and the structural changes upon strain has been carefully scrutinized at least for the bilayer material suggesting that the straightening of the Ni-O-Ni bond angles is related to the emergence of superconductivity in strained thin films [13]. As shown in Fig. 3(c,d), we find that compressive strain in $\text{La}_7\text{Ni}_5\text{O}_{17}$ also straightens the apical Ni-O-Ni bond angle. However, this trend is not systematic for the planar angles, as the inner layer of the trilayer tends to buckle slightly upon compressive strain, and so does one of the two inequivalent angles in the bilayer block. We note that the in-plane structural parameters for a -2% compressive strain approximately match the lattice constants obtained for a pressure of ~ 15 GPa, as shown in Fig. 3(a) (a pressure value that is also not fully in the tetragonal regime).

In Fig. 3(e-g), the band structures along high-symmetry directions and the corresponding Fermi surfaces are shown for $\text{La}_7\text{Ni}_5\text{O}_{17}$ for a -2% compressive strain. In order to make the comparison with pressure clearer, both of these cases are shown in $P4/mmm$ symmetry as this is the space group attained under pressure, as explained above. Once again, the band structure near the Fermi level is characterized by Ni- e_g (d_{z^2} and $d_{x^2-y^2}$) states, indicating that these two Ni- d orbitals still play the dominant role in the low-energy electronic structure of this material under strain. While the electronic structure is similar to that described under pressure, the d_{z^2} bonding bands are pushed down to lower energies so that at a -2% compressive strain, only the bilayer bonding band crosses it. The same effect has been shown in the isolated bilayer and trilayer RP phases under compressive strain from DFT calculations [31]. The electronic structure at this strain mimics better that obtained at 15 GPa (with some differences in band splittings), as shown in Appendix D – as mentioned above, the in-plane lattice constants also match those at 15 GPa, as shown in Fig. 3(a). The same applies to the hopping values obtained for a -2% strain that are lower than those obtained at 30 GPa and more similar instead to those derived at 15 GPa, as shown in Table I. Significantly lower values are obtained for t_{\perp}^z , as

expected, given the elongation of the c lattice constant upon compressive strain. The planar hoppings can instead be closely matched to the corresponding 15 GPa pressure. In the context of our electronic structure description, if superconductivity can be obtained upon strain in the 2323 RP nickelate polymorph $\text{La}_7\text{Ni}_5\text{O}_{17}$, it will be interesting to understand what role (if any) the extra corner pocket from the trilayer block might play for superconductivity when contrasting to pressure and also what the contributions of bilayer and trilayer blocks need to be in order for superconductivity to emerge.

Note added. During the completion of this work, evidence for superconductivity in $\text{La}_7\text{Ni}_5\text{O}_{17}$ -2323 was demonstrated by the authors of Ref. [44], as presented in the Frontiers of Unconventional Superconductivity Virtual Workshop (work unpublished).

IV. CONCLUSIONS

In summary, we have systematically studied the effects of pressure and biaxial compressive strain in the hybrid bilayer-trilayer (2323) RP nickelate $\text{La}_7\text{Ni}_5\text{O}_{17}$ via first-principles calculations. We have found that the structure of this hybrid nickelate at ambient pressure contains octahedral tilts, akin to the conventional trilayer and bilayer RP nickelates. Upon pressure, the structure becomes tetragonal, with the tilts of oxygen octahedra being completely suppressed at ~ 25 GPa. Under compressive strain, while the out-of-plane tilts are suppressed, the planar ones remain (at least up to the highest level of strain we have studied of -2%). The electronic structure of $\text{La}_7\text{Ni}_5\text{O}_{17}$ resembles a superposition of the conventional bilayer and trilayer RP components with some band shifts. At high pressures, an extra corner pocket of pure d_{z^2} character from the trilayer block emerges, but it is fragile as it can easily be shifted down to lower energies with a small U . This pocket is absent under compressive strain. If this hybrid system can be synthesized in bulk or thin film form, it would then be interesting to understand what role (if any) this extra corner pocket from the trilayer block can play for superconductivity.

ACKNOWLEDGEMENTS

We would like to thank Harry LaBollita for fruitful discussions. We acknowledge NSF grant No. DMR-2045826 and the ASU research computing center for HPC resources.

[1] H. Sun, M. Huo, X. Hu, J. Li, Z. Liu, Y. Han, L. Tang, Z. Mao, P. Yang, and B. Wang, Signatures of superconductivity near 80 K in a nickelate under high pressure, *Nature* **621**, 493 (2023).

[2] N. Wang, G. Wang, X. Shen, J. Hou, J. Luo, X. Ma, H. Yang, L. Shi, J. Dou, and J. Feng, Bulk high-temperature superconductivity in pressurized tetragonal $\text{La}_2\text{PrNi}_2\text{O}_7$, *Nature* **634**, 579 (2024).

- [3] J. Hou, P.-T. Yang, Z.-Y. Liu, J.-Y. Li, P.-F. Shan, L. Ma, G. Wang, N.-N. Wang, H.-Z. Guo, J.-P. Sun, Y. Uwatoko, M. Wang, G.-M. Zhang, B.-S. Wang, and J.-G. Cheng, Emergence of high-temperature superconducting phase in pressurized $\text{La}_3\text{Ni}_2\text{O}_7$ crystals, *Chin. Phys. Lett.* **40**, 117302 (2023).
- [4] Y. Zhu, D. Peng, E. Zhang, B. Pan, X. Chen, L. Chen, H. Ren, F. Liu, Y. Hao, N. Li, Z. Xing, F. Lan, J. Han, J. Wang, D. Jia, H. Wo, Y. Gu, Y. Gu, L. Ji, W. Wang, H. Gou, Y. Shen, T. Ying, X. Chen, W. Yang, H. Cao, C. Zheng, Q. Zeng, J. Guo, and J. Zhao, Superconductivity in pressurized trilayer $\text{La}_4\text{Ni}_3\text{O}_{10-\delta}$ single crystals, *Nature* **631**, 531 (2024).
- [5] Q. Li, Y.-J. Zhang, Z.-N. Xiang, Y. Zhang, X. Zhu, and H.-H. Wen, Signature of superconductivity in pressurized $\text{La}_4\text{Ni}_3\text{O}_{10}$, *Chin. Phys. Lett.* **41**, 017401 (2024).
- [6] M. Greenblatt, Ruddlesden-popper $\text{Ln}_{n+1}\text{Ni}_n\text{O}_{3n+1}$ nickelates: structure and properties, *Curr. Opin. Solid State Mater. Sci.* **2**, 174 (1997).
- [7] L. Wang, Y. Li, S.-Y. Xie, F. Liu, H. Sun, C. Huang, Y. Gao, T. Nakagawa, B. Fu, and B. Dong, Structure responsible for the superconducting state in $\text{La}_3\text{Ni}_2\text{O}_7$ at high-pressure and low-temperature conditions, *J. Am. Chem. Soc.* **146**, 7506 (2024).
- [8] J. Li, D. Peng, P. Ma, H. Zhang, Z. Xing, X. Huang, C. Huang, M. Huo, D. Hu, Z. Dong, X. Chen, T. Xie, H. Dong, H. Sun, Q. Zeng, H.-k. Mao, and M. Wang, Identification of superconductivity in bilayer nickelate $\text{La}_3\text{Ni}_2\text{O}_7$ under high pressure up to 100 GPa, *Nat. Sci. Rev.* **12**, nwaf220 (2025).
- [9] J. Li, C.-Q. Chen, C. Huang, Y. Han, M. Huo, X. Huang, P. Ma, Z. Qiu, J. Chen, X. Hu, L. Chen, T. Xie, B. Shen, H. Sun, D.-X. Yao, and M. Wang, Structural transition, electric transport, and electronic structures in the compressed trilayer nickelate $\text{La}_4\text{Ni}_3\text{O}_{10}$, *Sci. China Phys. Mech. Astron.* **67**, 117403 (2024).
- [10] M. Zhang, C. Pei, D. Peng, X. Du, W. Hu, Y. Cao, Q. Wang, J. Wu, Y. Li, H. Liu, C. Wen, J. Song, Y. Zhao, C. Li, W. Cao, S. Zhu, Q. Zhang, N. Yu, P. Cheng, L. Zhang, Z. Li, J. Zhao, Y. Chen, C. Jin, H. Guo, C. Wu, F. Yang, Q. Zeng, S. Yan, L. Yang, and Y. Qi, Superconductivity in trilayer nickelate $\text{La}_4\text{Ni}_3\text{O}_{10}$ under pressure, *Phys. Rev. X* **15**, 021005 (2025).
- [11] F. Li, Y. Hao, N. Guo, D. Jia, J. Dou, D. Peng, G. Zhang, L. Xiao, J. Zhang, W. Zhou, Y. Huang, X. Wang, Z. Guo, M. Mezouar, J. Elias F. S. Rodrigues, J. Luo, J. Yang, Q. Zeng, R. Zhou, H. Gou, Q. Zheng, G. Liu, and J. Zhang, Single-crystal structure determination of superconducting $\text{La}_4\text{Ni}_3\text{O}_{10-\delta}$ under high pressure, *Adv. Mater.* **37**, e07365 (2025).
- [12] E. K. Ko, Y. Yu, Y. Liu, L. Bhatt, J. Li, V. Thampy, C.-T. Kuo, B. Y. Wang, Y. Lee, K. Lee, J.-S. Lee, B. H. Goodge, D. A. Muller, and H. Y. Hwang, Signatures of ambient pressure superconductivity in thin film $\text{La}_3\text{Ni}_2\text{O}_7$, *Nature* **638**, 935 (2025).
- [13] L. Bhatt, A. Y. Jiang, E. K. Ko, N. Schnitzer, G. A. Pan, D. F. Segedin, Y. Liu, Y. Yu, Y.-F. Zhao, E. Abarca Morales, C. M. Brooks, A. S. Botana, H. Y. Hwang, J. A. Mundy, D. A. Muller, and B. H. Goodge, Resolving structural origins for superconductivity in strain-engineered $\text{La}_3\text{Ni}_2\text{O}_7$ thin films, *arXiv preprint arXiv:2501.08204* (2025).
- [14] M. Osada, C. Terakura, A. Kikkawa, M. Nakajima, H.-Y. Chen, Y. Nomura, Y. Tokura, and A. Tsukazaki, Strain-tuning for superconductivity in $\text{La}_3\text{Ni}_2\text{O}_7$ thin films, *Commun. Phys.* **8**, 251 (2025).
- [15] P. Li, G. Zhou, W. Lv, Y. Li, C. Yue, H. Huang, L. Xu, J. Shen, Y. Miao, W. Song, Z. Nie, Y. Chen, H. Wang, W. Chen, Y. Huang, Z.-H. Chen, T. Qian, J. Lin, J. He, Y.-J. Sun, Z. Chen, and Q.-K. Xue, Angle-resolved photoemission spectroscopy of superconducting $(\text{La,Pr})_3\text{Ni}_2\text{O}_7/\text{SrLaAlO}_4$ heterostructures, *Nat. Sci. Rev.* **12**, nwaf205 (2025).
- [16] G. Zhou, W. Lv, H. Wang, Z. Nie, Y. Chen, Y. Li, H. Huang, W. Chen, Y. Sun, Q.-K. Xue, and Z. Chen, Ambient-pressure superconductivity onset above 40 K in $(\text{La,Pr})_3\text{Ni}_2\text{O}_7$ films, *Nature* **640**, 641 (2025).
- [17] Y. Liu, E. K. Ko, Y. Tarn, L. Bhatt, J. Li, V. Thampy, B. H. Goodge, D. A. Muller, S. Raghu, Y. Yu, and H. Y. Hwang, Superconductivity and normal-state transport in compressively strained $\text{La}_2\text{PrNi}_2\text{O}_7$ thin films, *Nat. Mater.* **24**, 1221 (2025).
- [18] Z. Luo, X. Hu, M. Wang, W. Wú, and D.-X. Yao, Bilayer two-orbital model of $\text{La}_3\text{Ni}_2\text{O}_7$ under pressure, *Phys. Rev. Lett.* **131**, 126001 (2023).
- [19] Y. Zhang, L.-F. Lin, A. Moreo, and E. Dagotto, Electronic structure, dimer physics, orbital-selective behavior, and magnetic tendencies in the bilayer nickelate superconductor $\text{La}_3\text{Ni}_2\text{O}_7$ under pressure, *Phys. Rev. B* **108**, L180510 (2023).
- [20] Q.-G. Yang, D. Wang, and Q.-H. Wang, Possible s_{\pm} -wave superconductivity in $\text{La}_3\text{Ni}_2\text{O}_7$, *Phys. Rev. B* **108**, L140505 (2023).
- [21] Q.-G. Yang, K.-Y. Jiang, D. Wang, H.-Y. Lu, and Q.-H. Wang, Effective model and s_{\pm} -wave superconductivity in trilayer nickelate $\text{La}_4\text{Ni}_3\text{O}_{10}$, *Phys. Rev. B* **109**, L220506 (2024).
- [22] M. Zhang, H. Sun, Y.-B. Liu, Q. Liu, W.-Q. Chen, and F. Yang, s^{\pm} -wave superconductivity in pressurized $\text{La}_4\text{Ni}_3\text{O}_{10}$, *Phys. Rev. B* **110**, L180501 (2024).
- [23] H. Sakakibara, N. Kitamine, M. Ochi, and K. Kuroki, Possible high T_c superconductivity in $\text{La}_3\text{Ni}_2\text{O}_7$ under high pressure through manifestation of a nearly half-filled bilayer hubbard model, *Phys. Rev. Lett.* **132**, 106002 (2024).
- [24] V. Christiansson, F. Petocchi, and P. Werner, Correlated electronic structure of $\text{La}_3\text{Ni}_2\text{O}_7$ under pressure, *Phys. Rev. Lett.* **131**, 206501 (2023).
- [25] F. Lechermann, J. Gondolf, S. Bötzel, and I. M. Eremin, Electronic correlations and superconducting instability in $\text{La}_3\text{Ni}_2\text{O}_7$ under high pressure, *Phys. Rev. B* **108**, L201121 (2023).
- [26] Y. Zhang, L.-F. Lin, A. Moreo, T. A. Maier, and E. Dagotto, Prediction of s^{\pm} -wave superconductivity enhanced by electronic doping in trilayer nickelates $\text{La}_4\text{Ni}_3\text{O}_{10}$ under pressure, *Phys. Rev. Lett.* **133**, 136001 (2024).
- [27] Y. Zhang, L.-F. Lin, A. Moreo, T. A. Maier, and E. Dagotto, Structural phase transition, s^{\pm} -wave pairing, and magnetic stripe order in bilayered superconductor $\text{La}_3\text{Ni}_2\text{O}_7$ under pressure, *Nat. Commun.* **15**, 2470 (2024).
- [28] H. LaBollita, J. Kapeghian, M. R. Norman, and A. S. Botana, Electronic structure and magnetic tendencies of trilayer $\text{La}_4\text{Ni}_3\text{O}_{10}$ under pressure: Structural transition, molecular orbitals, and layer differentiation, *Phys. Rev. B* **109**, 195151 (2024).
- [29] C. Lu, Z. Pan, F. Yang, and C. Wu, Interlayer-coupling-driven high-temperature superconductivity in $\text{La}_3\text{Ni}_2\text{O}_7$

- under pressure, *Phys. Rev. Lett.* **132**, 146002 (2024).
- [30] J. Yang, H. Sun, X. Hu, Y. Xie, T. Miao, H. Luo, H. Chen, B. Liang, W. Zhu, G. Qu, C.-Q. Chen, M. Huo, Y. Huang, S. Zhang, F. Zhang, F. Yang, Z. Wang, Q. Peng, H. Mao, G. Liu, Z. Xu, T. Qian, D.-X. Yao, M. Wang, L. Zhao, and X. J. Zhou, Orbital-dependent electron correlation in double-layer nickelate $\text{La}_3\text{Ni}_2\text{O}_7$, *Nat. Commun.* **15**, 4373 (2024).
- [31] Y.-F. Zhao and A. S. Botana, Electronic structure of ruddlesden-popper nickelates: Strain to mimic the effects of pressure, *Phys. Rev. B* **111**, 115154 (2025).
- [32] F. Li, N. Guo, Q. Zheng, Y. Shen, S. Wang, Q. Cui, C. Liu, S. Wang, X. Tao, G.-M. Zhang, and J. Zhang, Design and synthesis of three-dimensional hybrid Ruddlesden-Popper nickelate single crystals, *Phys. Rev. Mater.* **8**, 053401 (2024).
- [33] X. Chen, Z. Zhang, A. S. Thind, S. Sharma, H. LaBollita, G. Peterson, H. Zheng, D. P. Phelan, A. S. Botana, R. F. Klie, and J. F. Mitchell, Polymorphism in the ruddlesden-popper nickelate $\text{La}_3\text{Ni}_2\text{O}_7$: Discovery of a hidden phase with distinctive layer stacking, *J. Am. Chem. Soc.* **146**, 6 (2024).
- [34] H. Wang, L. Chen, A. Rutherford, H. Zhou, and W. Xie, Long-range structural order in a hidden phase of ruddlesden–popper bilayer nickelate $\text{La}_3\text{Ni}_2\text{O}_7$, *Inorg. Chem.* **63**, 5020–5026 (2024).
- [35] P. Puphal, P. Reiss, N. Enderlein, Y.-M. Wu, G. Khal-iullin, V. Sundaramurthy, T. Priessnitz, M. Knauff, A. Suthar, L. Richter, M. Isobe, P. A. van Aken, H. Takagi, B. Keimer, Y. E. Suyolcu, B. Wehinger, P. Hansmann, and M. Hepting, Unconventional crystal structure of the high-pressure superconductor $\text{La}_3\text{Ni}_2\text{O}_7$, *Phys. Rev. Lett.* **133**, 146002 (2024).
- [36] S. Abadi, K.-J. Xu, E. G. Lomeli, P. Puphal, M. Isobe, Y. Zhong, A. V. Fedorov, S.-K. Mo, M. Hashimoto, D.-H. Lu, B. Moritz, B. Keimer, T. P. Devereaux, M. Hepting, and Z.-X. Shen, Electronic structure of the alternating monolayer-trilayer phase of $\text{La}_3\text{Ni}_2\text{O}_7$, *Phys. Rev. Lett.* **134**, 126001 (2025).
- [37] C. Huang, J. Li, X. Huang, H. Zhang, D. Hu, M. Huo, X. Chen, Z. Chen, H. Sun, and M. Wang, Superconductivity in monolayer-trilayer phase of $\text{La}_3\text{Ni}_2\text{O}_7$ under high pressure, *arXiv preprint arXiv:2510.12250* (2025).
- [38] M. Shi, D. Peng, K. Fan, Z. Xing, S. Yang, Y. Wang, H. Li, R. Wu, M. Du, B. Ge, Z. Zeng, Q. Zeng, J. Ying, T. Wu, and X. Chen, Pressure induced superconductivity in hybrid Ruddlesden–Popper $\text{La}_5\text{Ni}_3\text{O}_{11}$ single crystals, *Nat. Phys.* **21**, 1780 (2025).
- [39] V. Sundaramurthy, A. Suthar, P. Puphal, C. Le, Y. Gu, H. Yilmaz, P. Sosa-Lizama, P. A. van Aken, Y. E. Suyolcu, M. Isobe, A. P. Schnyder, X. Wu, M. Minola, B. Keimer, and M. Hepting, Comparative Raman study of Ruddlesden-Popper nickelates and the monolayer-trilayer polymorph, *arXiv preprint arXiv:2512.17583* (2025).
- [40] F. Lechermann, S. Bötzel, and I. M. Eremin, Electronic instability, layer selectivity, and fermi arcs in $\text{La}_3\text{Ni}_2\text{O}_7$, *Phys. Rev. Mater.* **8**, 074802 (2024).
- [41] Y. Zhang, L.-F. Lin, A. Moreo, T. A. Maier, and E. Dagotto, Electronic structure, self-doping, and superconducting instability in the alternating single-layer trilayer stacking nickelates $\text{La}_3\text{Ni}_2\text{O}_7$, *Phys. Rev. B* **110**, L060510 (2024).
- [42] H. LaBollita, S. Bag, J. Kapeghian, and A. S. Botana, Electronic correlations, layer distinction, and electron doping in the alternating single-layer–trilayer $\text{La}_3\text{Ni}_2\text{O}_7$ polymorph, *Phys. Rev. B* **110**, 155145 (2024).
- [43] S. Sharma, Y.-F. Zhao, and A. S. Botana, Structural stability, electronic structure, and magnetic properties of the single-layer trilayer $\text{La}_3\text{Ni}_2\text{O}_7$ polymorph, *Phys. Rev. B* **113**, 045139 (2026).
- [44] Z. Nie, Y. Li, W. Lv, L. Xu, Z. Jiang, P. Fu, G. Zhou, W. Song, Y. Chen, H. Wang, H. Huang, J. Lin, D. Shen, P. Li, Q.-K. Xue, and Z. Chen, Ambient-pressure superconductivity and electronic structures of engineered hybrid nickelate films, *arXiv preprint arXiv:2509.03502* (2025).
- [45] Y. Zhang, L.-F. Lin, A. Moreo, T. A. Maier, and E. Dagotto, Magnetic correlations and pairing tendencies of the hybrid stacking nickelate superlattice $\text{La}_7\text{Ni}_5\text{O}_{17}$ ($\text{La}_3\text{Ni}_2\text{O}_7/\text{La}_4\text{Ni}_3\text{O}_{10}$) under pressure, *Phys. Rev. B* **112**, 024508 (2025).
- [46] Z. Ouyang, R.-Q. He, and Z.-Y. Lu, Phase diagrams and two key factors to superconductivity of Ruddlesden-Popper nickelates, *Phys. Rev. B* **112**, 045127 (2025).
- [47] P. Giannozzi, S. Baroni, N. Bonini, M. Calandra, R. Car, C. Cavazzoni, D. Ceresoli, G. L. Chiarotti, M. Cococcioni, I. Dabo, A. Dal Corso, S. de Gironcoli, S. Fabris, G. Fratesi, R. Gebauer, U. Gerstmann, C. Gougoussis, A. Kokalj, M. Lazzeri, L. Martin-Samos, N. Marzari, F. Mauri, R. Mazzarello, S. Paolini, A. Pasquarello, L. Paulatto, C. Sbraccia, S. Scandolo, G. Sclauzero, A. P. Seitsonen, A. Smogunov, P. Umari, and R. M. Wentzcovitch, Quantum espresso: a modular and open-source software project for quantum simulations of materials, *J. Phys.: Condens. Matter* **21**, 395502 (2009).
- [48] P. Giannozzi, O. Andreussi, T. Brumme, O. Bunau, M. B. Nardelli, M. Calandra, R. Car, C. Cavazzoni, D. Ceresoli, M. Cococcioni, N. Colonna, I. Carnimeo, A. D. Corso, S. de Gironcoli, P. Delugas, R. A. D. Jr, A. Ferretti, A. Floris, G. Fratesi, G. Fugallo, R. Gebauer, U. Gerstmann, F. Giustino, T. Gorni, J. Jia, M. Kawamura, H.-Y. Ko, A. Kokalj, E. Küçükbenli, M. Lazzeri, M. Marsili, N. Marzari, F. Mauri, N. L. Nguyen, H.-V. Nguyen, A. O. de-la Roza, L. Paulatto, S. Poncé, D. Rocca, R. Sabatini, B. Santra, M. Schlipf, A. P. Seitsonen, A. Smogunov, I. Timrov, T. Thonhauser, P. Umari, N. Vast, X. Wu, and S. Baroni, Advanced capabilities for materials modelling with quantum espresso, *J. Phys.: Condens. Matter* **29**, 465901 (2017).
- [49] J. P. Perdew, K. Burke, and M. Ernzerhof, Generalized gradient approximation made simple, *Phys. Rev. Lett.* **77**, 3865 (1996).
- [50] We used the pseudopotentials `La.pbe-spfn-rrkjus_psl.1.1.0.0.UPF`, `Ni.pbe-spn-rrkjus_psl.1.1.0.0.UPF`, and `O.pbe-n-rrkjus_psl.1.1.0.0.UPF` from the Quantum ESPRESSO pseudopotential database: <https://www.quantum-espresso.org/pseudopotentials>.
- [51] T. Tadano, Y. Gohda, and S. Tsuneyuki, Anharmonic force constants extracted from first-principles molecular dynamics: applications to heat transfer simulations, *J. Phys.: Condens. Matter* **26**, 225402 (2014).
- [52] S. L. Dudarev, G. A. Botton, S. Y. Savrasov, C. J. Humphreys, and A. P. Sutton, Electron-energy-loss spectra and the structural stability of nickel oxide: An lsd+u study, *Phys. Rev. B* **57**, 1505 (1998).

Appendix A: Structural distortions from imaginary phonon modes

Figure. 4 demonstrates the lattice distortions associated with the five dynamically unstable modes of the $P4/mmm$ structure of $\text{La}_7\text{Ni}_5\text{O}_{17-2323}$ at ambient pressure. The most unstable mode, at -4.1 THz, has A_{1u} symmetry and is characterized by in-plane rotations within the inner layer of the trilayer, with NiO_6 octahedra rotating in opposite directions both within each layer and between vertically aligned octahedra in adjacent layers. The other four imaginary-frequency modes form two doubly degenerate E_u pairs at -3.1 THz and -2.1 THz. These modes involve antiphase octahedral tilts, in which adjacent octahedra tilt in opposite directions within the corner-sharing octahedral framework. Within each degenerate pair, the two modes correspond to symmetry-related octahedral tilting patterns. The -3.1 THz modes exhibit stronger distortions in the trilayer, whereas the -2.1 THz modes show larger distortions in the bilayer. The bilayer-trilayer tilting correlation is reversed between the -3.1 and -2.1 THz modes.

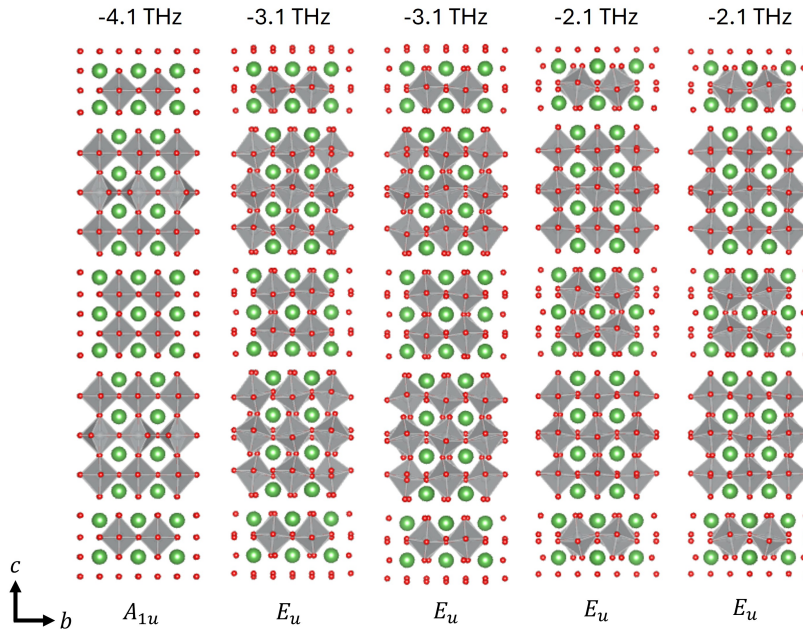


FIG. 4. Distortions based on the eigenvectors of the phonon modes with imaginary frequencies (labeled on top) at ambient pressure for $\text{La}_7\text{Ni}_5\text{O}_{17-2323}$ in $P4/mmm$ symmetry. The corresponding irreducible representations are labeled at the bottom.

Appendix B: Evolution of the phonon dispersion in $P4/mmm$ symmetry with pressure

Figure. 5 demonstrates the evolution of the phonon dispersion of $\text{La}_7\text{Ni}_5\text{O}_{17-2323}$ in $P4/mmm$ symmetry with pressure. At ambient pressure, one A_{1u} mode and two doubly degenerated E_u modes exhibit imaginary frequencies, as explained in the main text. At 20 GPa only the the A_{1u} mode associated with in-plane rotations remains imaginary. Consistently, the structure with lowest electronic energy at 20 GPa shows in-plane octahedra rotations without cross-plane tilting. At 30 GPa, the phonon dispersion demonstrates no imaginary frequencies, confirming the dynamical stability of the $P4/mmm$ phase at 30 GPa.

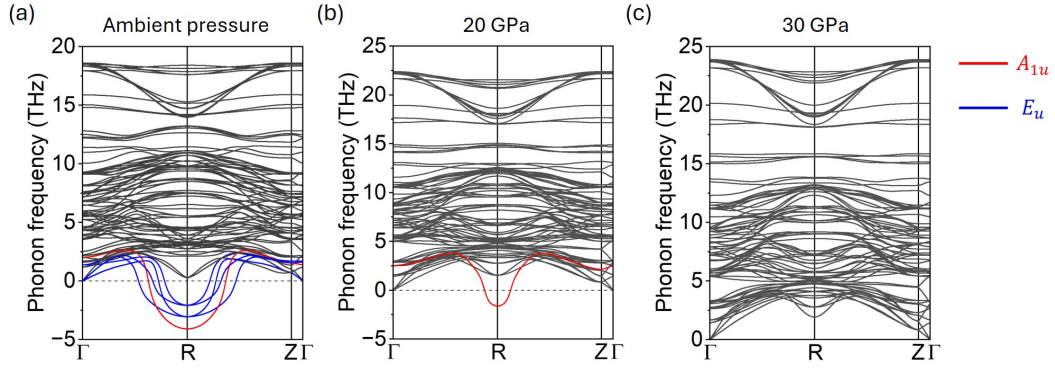


FIG. 5. Phonon dispersion of $\text{La}_7\text{Ni}_5\text{O}_{17-2323}$ in $P4/mmm$ symmetry under (a) ambient pressure, (b) 20 GPa, and (c) 30 GPa.

Appendix C: Electronic structures considering DFT+ U

The electronic structure for $\text{La}_7\text{Ni}_5\text{O}_{17-2323}$ in $P4/mmm$ symmetry with a $U = 4.7$ eV under 30 GPa, and -2% biaxial strain is shown in Fig. 6, and Fig. 7, respectively. The DFT+ U calculations were performed using the Dudarev formulation [52]. A Hubbard U of 4.7 eV was applied to Ni-3d manifold. Considering DFT+ U shifts the d_{z^2} bands to lower energy.

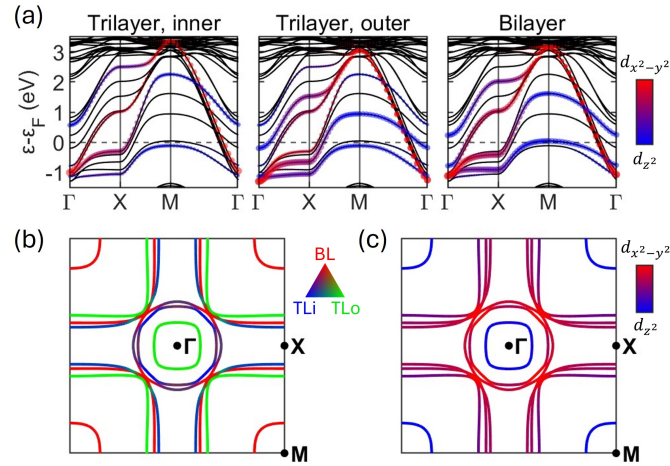


FIG. 6. Electronic structure of $\text{La}_7\text{Ni}_5\text{O}_{17-2323}$ in $P4/mmm$ symmetry under 30 GPa with $U = 4.7$ eV. (a) Electronic band structure. (b,c) Fermi surface cutoff at the $k_z = 0$ plane. The color scale represents contributions from different Ni orbitals or sites.

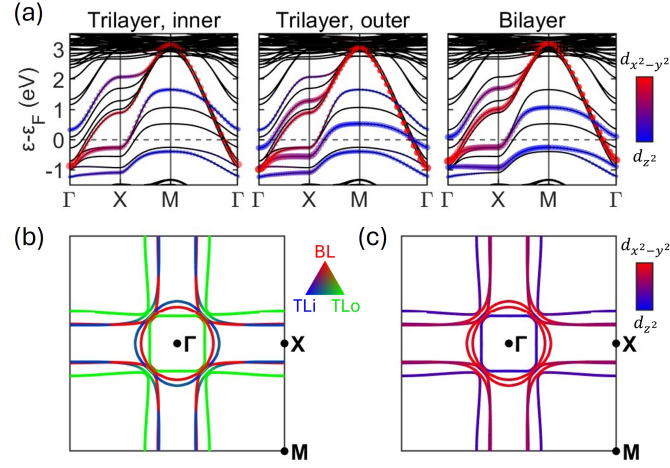


FIG. 7. Electronic structure of $\text{La}_7\text{Ni}_5\text{O}_{17-2323}$ in $P4/mmm$ symmetry under a -2% biaxial compressive strain with $U = 4.7$ eV. (a) Electronic band structure. (b,c) Fermi surface cutoff at the $k_z = 0$ plane. The color scale represents contributions from different Ni orbitals or sites.

Appendix D: Electronic structure at 15 GPa

Figure 8 shows the electronic structure of $\text{La}_7\text{Ni}_5\text{O}_{17-2323}$ in $P4/mmm$ symmetry at 15 GPa, which mimics closely the lattice constants obtained under a -2% compressive biaxial strain.

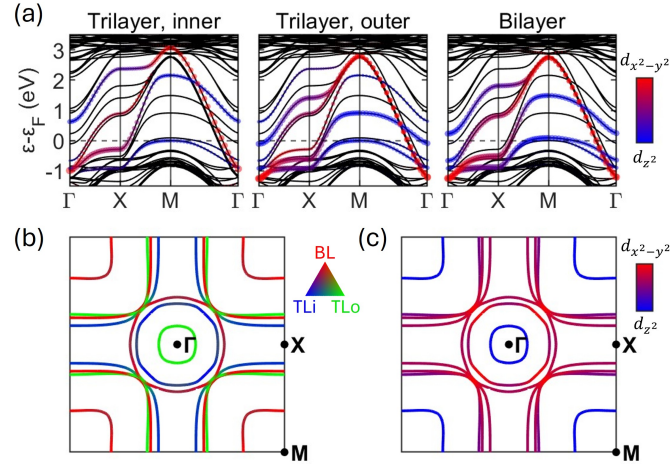


FIG. 8. Electronic structure of $\text{La}_7\text{Ni}_5\text{O}_{17-2323}$ in $P4/mmm$ symmetry under 15 GPa. (a) Electronic band structure. (b,c) Fermi surface cutoff at the $k_z = 0$ plane. The color scale represents contributions from different Ni orbitals or sites.